Molecular Systems Biology (2006) doi:10.1038/msb4100098

www.molecularsystemsbiology.com
Article number: 57

molecular systems biology

Cell lineage transport: a mechanism for molecular gradient formation

Marta Ibañes[1,3], Yasuhiko Kawakami[1], Diego Rasskin-Gutman[1,4] and Juan Carlos Izpisúa Belmonte[1,2,*]

[1] Gene Expression Laboratory, Salk Institute for Biological Studies, La Jolla, CA, USA and [2] Center of Regenerative Medicine in Barcelona, Barcelona, Spain
[3] Present address: Department Estructura i Constituents de la Matèria, University of Barcelona, Diagonal 647, Barcelona 08028, Spain
[4] Present address: Institute Cavanilles for Biodiversity and Evolutionary Biology, University of Valencia, Apartado Postal 22085, 46071 Valencia, Spain
* Corresponding author. Gene Expression Laboratory, Salk Institute for Biological Studies, 10010 North Torrey Pines Rd, La Jolla, CA 92037, USA
Tel.: +1 8584534100x1130; Fax: +1 8584532573; E-mail: belmonte@salk.edu

Received 27.2.06; accepted 18.8.06

Gradient formation is a fundamental patterning mechanism during embryo development, commonly related to secreted proteins that move along an existing field of cells. Here, we mathematically address the feasibility of gradients of mRNAs and non-secreted proteins. We show that these gradients can arise in growing tissues whereby cells dilute and transport their molecular content as they divide and grow, a mechanism we termed 'cell lineage transport.' We provide an experimental test by unveiling a distal-to-proximal gradient of *Hoxd13* in the vertebrate developing limb bud driven by cell lineage transport, corroborating our model. Our study indicates that gradients of non-secreted molecules exhibit a power-law profile and can arise for a wide range of biologically relevant parameter values. Dilution and nonlinear growth confer robustness to the spatial gradient under changes in the cell cycle period, but at the expense of sensitivity in the timing of gradient formation. We expect that gradient formation driven by cell lineage transport will provide future insights into understanding the coordination between growth and patterning during embryonic development.
Molecular Systems Biology 17 October 2006; doi:10.1038/msb4100098
Subject Categories: simulation and data analysis; development
Keywords: cell division and growth; dilution; molecular dynamics modeling; molecular gradients; non-secreted molecules; limb development

Introduction

Molecules distributed along gradient profiles have been repeatedly observed during embryonic development in a variety of multicellular organisms. Known examples include, in *Drosophila*, bicoid, decapentaplegic (dpp), hedgehog and wingless (Driever and Nusslein-Volhard, 1988a, b; Teleman and Cohen, 2000; Tabata, 2001; Martinez-Arias, 2003; Ephrussi and St Johnston, 2004); in *Xenopus*, Activin (Green, 2002); in mouse and chick, fibroblast growth factor 8 (fgf8) (Dubrulle and Pourquié, 2004); and Auxin in *Arabidopsis* (Bhalerao and Bennett, 2003). Gradients of secreted molecules (morphogens) have been proposed as a morphogenetic mechanism that can pattern the early embryo by conferring positional information to the cells, eliciting different responses according to concentration thresholds (Turing, 1952; Wolpert, 1969; Driever and Nusslein-Volhard, 1988b; Lawrence and Struhl, 1996; Gurdon and Bourillot, 2001; Lawrence, 2001). Indeed, gradients of the transcription factor bicoid in the *Drosophila* syncytium and the secreted protein dpp have been reported to act in such a morphogen-like manner (Driever and Nusslein-Volhard, 1988b; Teleman and Cohen, 2000; Ephrussi and St Johnston, 2004).

The most widely recognized mechanism for protein gradient formation is the secretion of a protein that passively diffuses away from its source of production (Crick, 1970). However, several concerns have been raised about the ability of a protein to effectively form a gradient through passive diffusion alone because diffusion may be hampered by the insolubility of ligands and their interaction with receptors (Kerszberg and Wolpert, 1998; Teleman *et al*, 2001; Lander *et al*, 2002; Vincent and Dubois, 2002; Kruse *et al*, 2004; Mann and Culi, 2005). As a result, and according to several observations (e.g., the intracellular accumulation of ligands in vesicles), active protein transport mechanisms have been proposed such as transcytosis (Entchev *et al*, 2000; Strigini and Cohen, 2000; Pfeiffer *et al*, 2002), cytoneme-mediated (Ramirez-Weber and Kornberg, 1999), and vesicle or lipoprotein transport (Greco *et al*, 2001; Panakova *et al*, 2005; Tanaka *et al*, 2005). These transport mechanisms have been also analyzed computationally and mathematically (Kerszberg and Wolpert, 1998; Eldar *et al*, 2002, 2003; Lander *et al*, 2002; Kruse *et al*, 2004; Bollenbach *et al*, 2005; Shimmi *et al*, 2005), generating new perspectives on the role of diffusion and on the nature and formation of molecular gradients.

The common denominator of all the above-mentioned gradient formation dynamics is the spatial transport of the protein by means of a specific molecular mechanism (e.g., passive diffusion, active transport through vesicles, etc.) over the underlying field of cells. Other transport mechanisms could involve cells acting as active molecular carriers through cell proliferation, cell growth, or cell migration (Lecuit and Cohen, 1998; Tabata, 2001; Teleman *et al*, 2001). For example, it has been found that cells dividing and leaving the *wingless* expression domain in *Drosophila* embryos retain the inherited wingless protein in secretory vesicles and carry them over distances of several cell diameters (Pfeiffer *et al*, 2000). Furthermore, it has been proposed that molecular decay coupled to these transport mechanisms could elicit molecular gradients (Gaunt *et al*, 2003; Dubrulle and Pourquié, 2004; Gaunt, 2004). Indeed, it has been shown that mRNAs can be distributed in a gradient profile formed by the mRNA decay in tissues with polarized growth (Dubrulle and Pourquié, 2004).

All these data point towards the importance of cell-driven molecular transport mechanisms for gradient formation during morphogenesis (Zhu and Scott, 2004). However, a full characterization, involving mathematical analyses and further experimental evidence, of the dynamics of gradient formation based on such transport processes is missing. Specifically, the implications of cell division and cell growth dynamics in the formation of gradients of non-secreted proteins and mRNAs have not been studied yet. Herein we focus on the dilution and transport of mRNAs and non-secreted proteins driven by cell division and cell growth dynamics, a mechanism we call 'cell lineage transport.' Gradients driven by 'cell lineage transport' emerge under several specific conditions, which we will explore in this paper, involving particular dynamics of tissue growth coupled with a local source of mRNA transcription. To characterize this mechanism for gradient formation, we introduce a computational model, supporting it with novel *in vivo* data on mRNA gradients. In addition, we extend our model to gradients formed by molecular decay in growing tissues (Dubrulle and Pourquié, 2004), which do not involve clonal dilution, comparing them with gradients driven by cell lineage transport. Our mathematical analysis shows that both mRNAs and non-secreted proteins can form a gradient through cell lineage transport and unveils the dynamics and features of their gradient profiles.

Results

A framework for mRNA and protein gradient formation through cell lineage transport

We characterized a basic scenario for the formation of gradients of mRNA and non-secreted proteins through cell lineage transport (Figure 1). In this scenario, when a cell divides, the daughter cells inherit, on average, half the amount of mRNA and protein of its progenitor, diluting its molecular content. Cell descendants rapidly grow after dividing to reach the diameter l of the progenitor cell, carrying their molecular content along the same spatial axis.

In our model, we also assumed that only a group of N cells situated in one of the tips of the growing tissue (hereafter called 'domain of transcription (DoT)') transcribes mRNA, such that a constant amount of mRNA is maintained in the transcribing cells. In addition, protein is translated in all cells

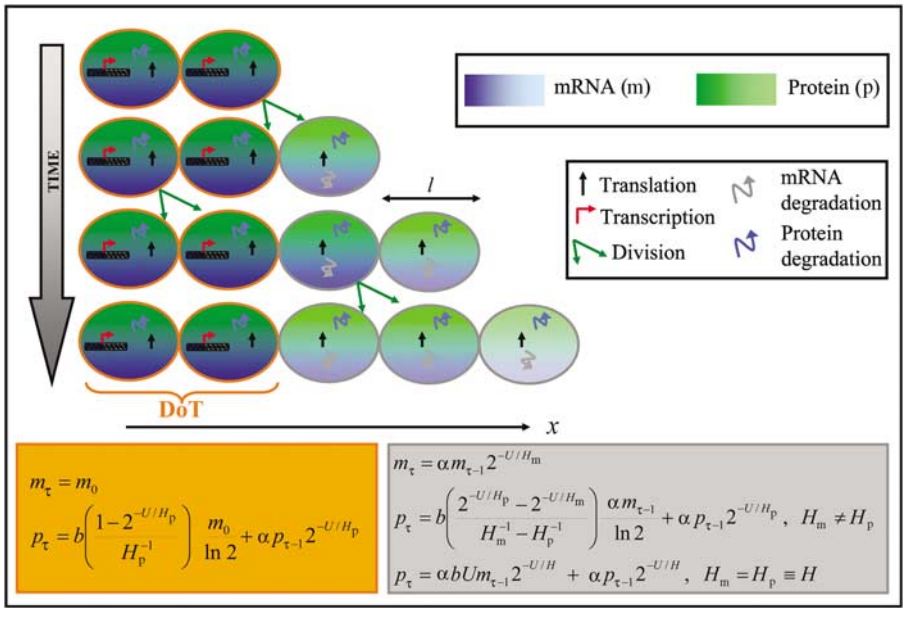

Figure 1 A model for gradient formation driven by cell lineage transport. Cells divide and grow, eliciting the outgrowth of tissue along the *x*-axis. Cells dilute and transport their molecular content when dividing (green arrows). A pool of N cells transcribes (red arrow) mRNA and constitutes the DoT. In the panel, the pool has two cells (in orange, $N=2$). Outside the DoT, the mRNA is only degraded (twisted gray arrow), whereas the protein is translated and degraded (black and twisted blue arrows, respectively). The equations characterizing the molecular dynamics at time intervals U proportional to the duration of the cell cycle, Cc, are detailed. Equations describe the (m) mRNA and (p) protein content of a cell at time $t_\tau = \tau U$ when it is located (orange) inside and (gray) outside the DoT. This cell inherited a fraction α of its progenitor's molecular content at time $t_{\tau-1}=(\tau-1)U$. The cell spatial dynamics are detailed in Supplementary information. m_0, b and $H_{m,p}$ denote the amount of mRNA at the DoT, the protein translation rate and the mRNA and protein half-lives, respectively.

containing mRNA proportionally to their amount of mRNA. The mRNA and protein turnovers were also included, as indicated by their half-lives (H_m and H_p for the mRNA and protein, respectively).

In order to characterize this gradient formation dynamics, we elaborated on a novel computational model, using a time-discrete modeling approach, which could include cells dividing in synchrony (Supplementary information).

According to the dynamics described, the molecular content in a cell becomes spatially transported when the cell is displaced and it evolves over time due to dilution, molecular decay, protein translation and mRNA transcription. Therefore, in the presence of a localized source of mRNA with proliferating and growing cells (the DoT), we expected the formation of mRNA and non-secreted protein gradients.

mRNA and protein gradients formed by cell lineage transport

Our computational analysis showed that, following the cell lineage transport dynamics, mRNA gradients with a maximum at the DoT and a decreasing minimum at the opposite end of the growing tissue are formed (Figure 2A–C). Note that these mRNA cell lineage gradients are characterized by two overlapping, but distinct in size, spatial domains (Figure 2D). The large domain is the spatial region over which the gradient is formed. The small domain is the DoT. Importantly, these two domains can be detected experimentally (Dubrulle and Pourquié, 2004). Transcription synthesizes from DNA premature mRNA, which contains both exonic and intronic sequences. These transcripts are then spliced such that mature mRNA, which contains only exonic sequences, is formed. Therefore, probes directed against intronic sequences detect the nascent transcripts and can be used to mark the DoT. In contrast, the exonic expression domain spans over those cells containing mature mRNA above a threshold, detecting the spatial region where the gradient is formed (Figure 2D). Therefore, *in vivo*, cell lineage gradients will exhibit graded exonic expression domains, which span more broadly than the intronic domain.

Our mathematical analysis indicated that mRNA cell lineage gradients have an average spatial profile, which is steepest at times just before the next cell division occurs (Supplementary information). Specifically, mRNAs have a power-law profile, with no characteristic length, due to the nonlinear growth of the tissue (Materials and methods). Neither the level of synchrony of the cell cycle between cells, nor fluctuations in the duration of the cell cycle and molecular amount inherited

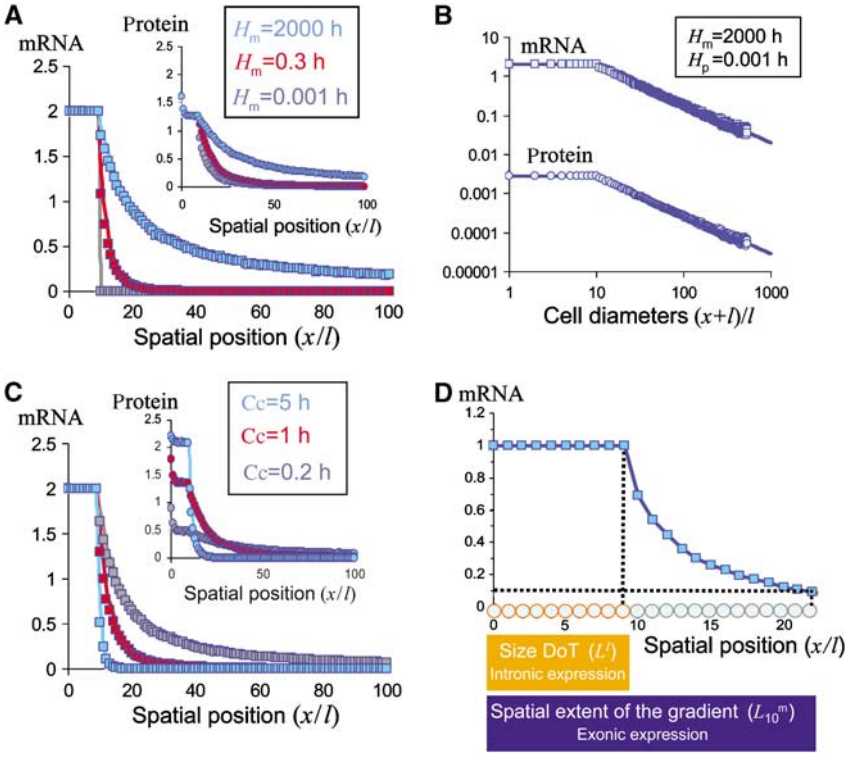

Figure 2 mRNA and protein gradients driven by cell lineage transport. Numerical gradients are represented by symbols (squares for mRNAs and circles for proteins). Lines are the continuous analytical profiles (Materials and methods). (**A**) mRNA and protein gradients for three different mRNA half-lives, H_p=0.7 h and Cc=1 h (gray, H_m=0.001 h). For very unstable mRNAs, a protein, but not an mRNA, gradient can be formed (red, H_m=0.3 h). For intermediate mRNA half-lives, mRNA and protein gradients are shaped by both the molecular decay and the dilution process (blue, H_m=2000 h). For very stable mRNAs, clonal dilution forms mRNA gradients. (**B**) mRNA and protein gradients in logarithmic scales for very unstable proteins (H_p=0.001 h). These protein gradients exhibit the same spatial decay as the mRNA, with very small protein amounts. Parameter values are H_m=2000 h and Cc=1 h. (**C**) mRNA and protein gradients for decreasing durations of the cell cycle: (blue) Cc=5 h, (red) Cc=1 h, (gray) Cc=0.2 h, for H_m=0.5 h and H_p=0.8 h. Gradients become steeper for slower cell cycles. In panels A–C, parameter values are N=10, m_0=2, b=1 and α=1/2 and numerical gradients are averaged over 10^3 simulations with stochastic cell cycles (Supplementary information). (**D**) (Orange) Spatial extent of the DoT (L^I=Nl) and (blue) spatial domain over which the (squares) mRNA gradient decays 10-fold (L_{10}^m). Cells are denoted by circles (encircled in orange inside the DoT and in gray outside it). Exonic and intronic probes can be used to detect the spatial region where the gradient spans and the DoT, respectively.

by each cell descendant alters this profile significantly (Supplementary information).

We obtained similar dynamics for non-secreted proteins, which also become distributed along gradients (Figure 2A–C). Experimentally, these gradients will show a protein expression domain, spanning over the whole gradient, larger than the intronic domain of expression. Our analysis indicated that the average gradient profile for proteins is characterized by a combination of power-like decays modulated by the mRNA and protein half-lives (Materials and methods). In the absence of an mRNA distribution (i.e. the mRNA is located only at the DoT), non-secreted proteins can form a gradient (Figure 2A; Materials and methods). In addition, when the mRNA forms a gradient, the protein is always distributed in a graded profile (Figure 2B).

In our model, cells reach a specific position outside the DoT after an average constant number of divisions, independently of how fast the cell cycle is. Thus, at this spatial position, the molecular content has decayed through dilution in the same proportion for fast and slow cell cycles. However, cells with faster cell cycles reach this position earlier and, as molecules degrade over time, contain more molecular content. Accordingly, our results showed that mRNA and protein gradients become steeper as the mRNA half-life is reduced or the cell cycle lasts longer (Figure 2A and C). In addition, longer protein half-lives make protein gradients shallower (Figure 2A and B; Materials and methods). Thus, extremely short mRNA half-lives compared to the cell cycle do not give rise to mRNA gradients, but protein gradients can still be formed if the protein is stable enough (Figure 2A).

Spatial properties of gradients driven by cell lineage transport

Molecular gradients in developing embryos should vary significantly in order to elicit different responses and thus be biologically relevant. Specifically, gradients with 10-fold variations along the overlying field of cells have been measured in different scenarios (Entchev *et al*, 2000; Houchmandzadeh *et al*, 2002; Dubrulle and Pourquié, 2004). Accordingly, we focused on the features of cell lineage gradients with 10-fold decays and defined the spatial extent of the gradient ($L_{10}^{m,p}$) as the space occupied by all those cells with an amount of mRNA/protein equal to or higher than 10% of the amount at the DoT (Figure 2D; Materials and methods). Note that, as indicated, the exonic/protein expression domain will span over this domain, whereas the intronic expression will extend over the DoT. Thus, by mathematically computing the ratio between the spatial extent of the mRNA gradient and the size of the DoT (L_{10}^{m}/L^{I}; hereafter called differential expression), we could characterize the differential exonic and intronic domains of expression that are expected for cell lineage gradients (Table I). When only the cells at the DoT contain mRNA and, hence, no mRNA gradient is formed, there is no differential expression ($L_{10}^{m}/L^{I}=1$) and the exonic and intronic domains of expression will span over the same spatial region.

As shown in Table I, the differential expression depends on the parameter $\gamma_m \equiv H_m/Cc$ alone, which we defined as the 'relative half-life' of the mRNA, as it measures the mRNA half-life compared to the duration of the cell cycle (i.e. large/small relative half-lives correspond to molecular half-lives much longer/shorter than the cell cycle). Our results indicated that the differential expression increases with the relative half-life until it is saturated (Figure 3A). Even if the mRNA half-life is rather shorter than the cell cycle length, a differential expression can arise (Figure 3A–C). For molecular decays that are not significant, mRNA gradients are still formed owing to the process of dilution inherent in cell proliferation. In this case, the gradients have a maximum extension proportional to the size of the DoT (Figure 3A). In addition, long-range mRNA gradients can arise for a wide range of values of the relative molecular half-lives (Figure 3A–C).

Table I Mathematical expressions for gradients created by cell lineage transport

Differential expression of the gradient	$L_{10}^{m,p}/L^{I} = 10^{1/(1+Cc/H_{m,p})}$
Average number of cell divisions per cell to form a gradient	$ND_{10}^{m,p} = \frac{\log_2 10}{1+Cc/H_{m,p}}$
Time to form a gradient	$t_{m,p} = H_{m,p} Cc \frac{\log_2 10}{Cc+H_{m,p}}$

For proteins, these expressions apply only when the protein gradient is formed by very short-lived mRNAs (Materials and methods).

Our results indicated that protein gradients, arising from either mRNA gradients or non-graded mRNAs, behave in a similar manner qualitatively and thus can be characterized equivalently (Materials and methods).

Temporal properties of gradients driven by cell lineage transport

As gradients created by cell lineage transport are formed as more and more cycles of cell division occur, and thus as a function of time, it was also important to know how many cell divisions and how long these gradients need to be formed (Materials and methods).

We found that the average number of cell divisions required to form a gradient with a 10-fold decay is rather small and saturated for large relative half-lives (Table I and Supplementary Figure S2A). Our results also indicated that the time gradients take to be formed ranges from minutes to hours depending on the specific values of the molecular half-lives and the duration of the cell cycle (Table I and Figure 4A). This time depends only on the duration of the cell cycle and thus on how fast the tissue grows for large relative half-lives, whereas the molecular half-life controls the time of gradient formation for small relative half-lives (Figure 4A).

Our numerical results showed that gradients formed by cell lineage transport are maintained as long as the tissue is growing and the cell lineage transport is active: once the tissue stops growing, no transport or dilution takes place. Thus, these gradients disappear in a time period controlled by the molecular dynamics alone.

Cell lineage transport gradients can be formed within large parameter ranges that are biologically relevant

We computed for which parameter values mRNA and protein gradients with a 10-fold decay over a spatial region

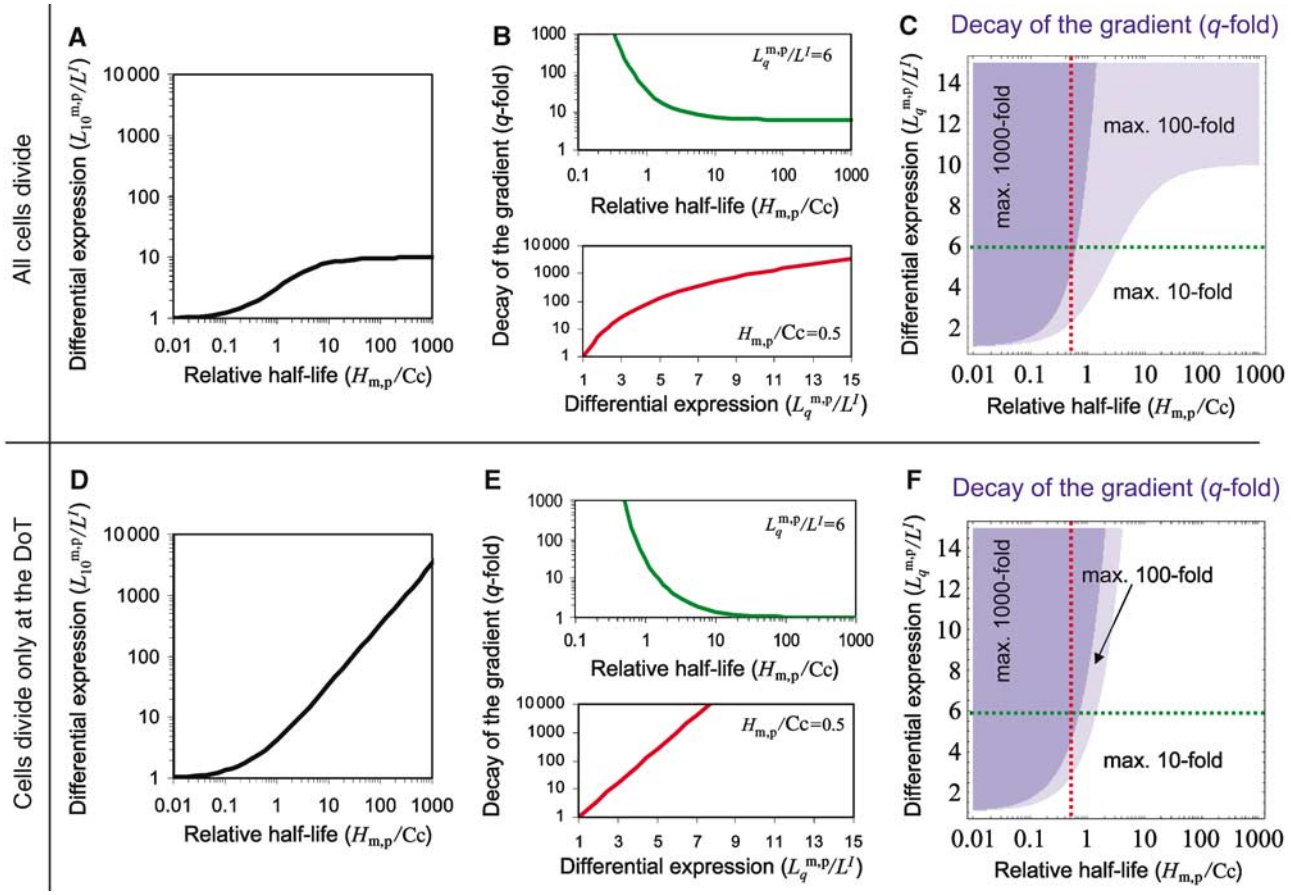

Figure 3 Spatial properties of mRNA and protein gradients. In the case of proteins, results are shown only for protein gradients formed by mRNAs with very small relative half-lives. (**A–C**) Properties of cell lineage transport gradients, involving clonal dilution. (**D–F**) Results for gradients formed when only the cells at the DoT divide (there is no repeated dilution) asynchronously. (A, D) For a 10-fold decay gradient, ratio between the extent of the gradient and the size of the DoT ($L_{10}^{m,p}/L^l$, differential expression) for different values of the relative half-life. In panel A, the gradient reaches a maximum extension. (B, E, top) As a function of the relative half-life, *q*-fold decay of the gradient at a distance six times longer than the DoT ($L^{m,p}/L^l$=6). In panel E, there is no decay for large relative half-lives. (B, E, bottom) Decay of the gradient as a function of the distance from the DoT (measured by the ratio $L^{m,p}/L^l$) for $H_{m,p}$/Cc=0.5. At larger distances, the decay is larger. In panel E, the dependence is linear. (C, F) Parameter regions where the mRNA or protein gradient decays at most (white) 10-fold, (light blue) 100-fold or (dark blue) 1000-fold, as a function of the relative half-lives (logarithmic scale) and the differential expression ($L^{m,p}/L^l$). The gradient decay along the green and red dotted lines is detailed in panels B and E (top) and panels B and E (bottom), respectively.

at least 50% larger than the DoT and not requiring many cell divisions can be produced. We found that mRNA and protein gradients satisfying these conditions can arise in a very large region of the parameter space, which extends to smaller relative half-lives if the molecular content varies largely (100-fold; Figure 4B). In the case of proteins, the ranges of relative half-lives that can elicit protein gradients are much larger, because, as indicated, protein gradients are created even if either the mRNA or the protein relative half-life is very small.

In eukaryotic cells, the half-life of mRNAs varies between seconds and hours, whereas the time between divisions varies between minutes and several hours (Peltz *et al*, 1991; Sachs, 1993; Ross, 1995; Varshavsky, 1996; Figueroa *et al*, 2003). As shown in Figure 4B, our results indicated that these biological timescales allow for the formation of mRNA and protein gradients by cell lineage transport in several developmental contexts, both for very short and long molecular half-lives and cell cycles.

Molecular dilution can confer robustness to the spatial gradient

We analyzed a particular case of the model in which only the mRNA transcribing cells could divide (Supplementary information). For this tissue dynamics, cells outside the DoT just transport their molecular content when being displaced by proliferating cells at the DoT. As before, we considered that the mRNA and the protein are degraded, and the protein can be translated in cells outside the DoT. However, in contrast with the dynamics described so far, this case scenario did not involve clonal dilution, as cells outside the DoT cannot divide.

Our analysis revealed that the molecular turnover becomes essential for the formation of gradients in this tissue dynamics, as previously proposed (Dubrulle and Pourquié, 2004). As this scenario applies to *fgf8* gradients formed by molecular decay in the presomitic mesoderm of chick and mouse embryos (Dubrulle and Pourquié, 2004), we confirmed that our model

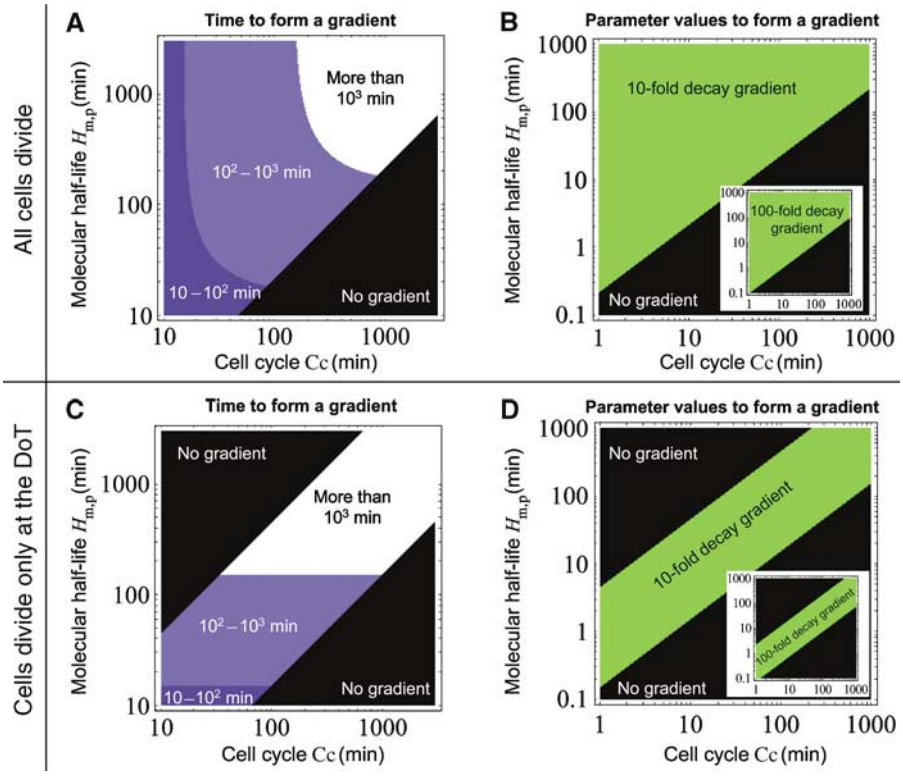

Figure 4 Timing and parameter space of mRNA and protein gradients. In the case of proteins, results apply only for protein gradients formed by very short-lived mRNAs. (**A, B**) Analytical results for cell lineage transport gradients, with clonal dilution. (**C, D**) Analytical results in the absence of repeated dilution. (A, C) Parameter space of molecular half-lives ($H_{m,p}$) and durations of the cell cycle (Cc) where the time of gradient formation is between (dark blue) 10 and 100 min, (light blue) 100 and 1000 min, and (white) longer than 1000 min. (B, D) (green) Parameter space of molecular half-lives ($H_{m,p}$) and durations of the cell cycle (Cc) that lead to gradients with a 10-fold decay over a region 1.5 longer than the DoT ($L_{10}^{m,p}/L^{l} > 1.5$) and requiring at most 15 divisions on average per cell ($ND_{10}^{m,p} \leqslant 15$). The equivalent analysis applied to 100-fold decaying gradients is depicted in the insets. In all panels, the parameter regions where no gradients are formed ($L_{10}^{m}/L^{l} \leqslant 1.5$ and $ND^{m,p} > 15$) are shown in black. Note the appearance of new black domains in panels C and D. In these domains, the molecular content spans too Llp1.5 homogeneously, with no significant decay. Scales are logarithmic.

for this tissue dynamics could appropriately reproduce these experimental data (Supplementary information).

An analysis of the gradients arising when only the cells at the DoT divided revealed that the absence of proliferating cells outside the DoT, and thus the absence of clonal dilution, changes many of the properties of the molecular gradients. Owing to the linear growth involved in this tissue dynamics, the gradient profile becomes exponential with a characteristic length proportional to the relative molecular half-lives and to the size of the DoT (Supplementary information). Hence, in this case, the length of the gradient and the number of divisions can increase indefinitely as the relative half-life augments (Figure 3D and Supplementary Figure S2B). Compared to gradients driven by cell lineage transport, the differential expression is larger and a higher average number of cell divisions per cell and longer times are required (Figures 3D and 4C, and Supplementary Figure S2B). Accordingly, when taking into account that cells can divide only a limited number of times (Conlon and Raff, 1999), we obtained that above a maximum relative half-life the molecular content spans too homogeneously and does not form a gradient (Figure 3E and F, and Supplementary Figure S2B). Therefore, in the absence of successive dilutions, the molecular half-lives cannot be arbitrarily long compared to the cell cycle duration in order to form a gradient with a relevant decay, and thus gradient formation occurs in a smaller parameter region (Figure 4D).

Robustness of gradients can be analyzed through its sensitivity to parameter changes (Eldar *et al*, 2003; Bollenbach *et al*, 2005; Materials and methods). Specifically, we focused on the sensitivity of the differential expression and the timing of gradient formation to variations in the duration of the cell cycle, as changes in the temperature at which an embryo is developing alter the duration of the cell cycle but do not necessarily induce patterning defects. Our results showed that each mechanism exhibits very different behaviors. First, gradients formed by cell lineage transport, involving repeated dilution owing to successive cell divisions, have a less sensitive differential expression when the cell cycle is altered (Figure 5A and B). Specifically, the differential expression and thus the average number of cell divisions involved in the gradient become robust for large relative half-lives (Figure 5A; data not shown). Second, for gradients formed when only the cells at the DoT divide, the time of formation is independent of the duration of the cell cycle (Table I, Figure 4C and Supplementary information), in contrast with the timing of cell lineage gradients, which is very sensitive to variations in the cell cycle (Figure 5C). Note that at large relative half-lives,

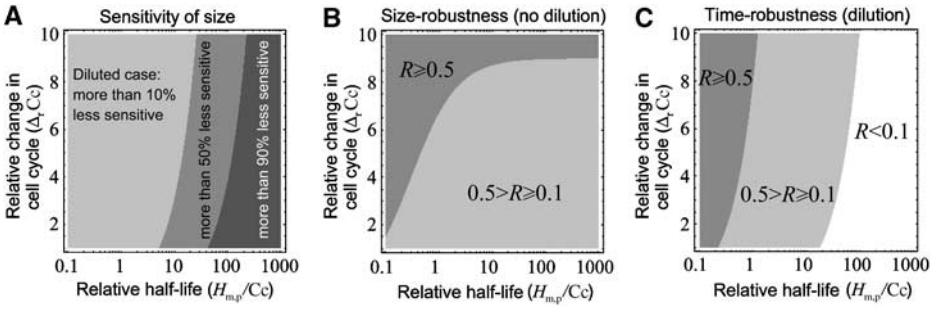

Figure 5 Robustness of mRNA and protein gradients to changes in the cell cycle. (**A**) Decrease in the sensitivity of the differential expression owing to dilution as a function of the change in the cell cycle and for a wide range of relative half-lives. This change is measured by the ratio S_d/S_{nd} (Materials and methods). Parameter domains eliciting (light gray) $S_d/S_{nd} \in (0.5, 0.9)$, (gray) $S_d/S_{nd} \in (0.1, 0.5)$ and (dark gray) $S_d/S_{nd} \leqslant 0.1$ are depicted. (**B**) Robustness of the differential expression when only the cells at the DoT divide asynchronously. (**C**) Robustness in the timing of gradient formation for tissue dynamics involving evenly proliferating cells. In panels B and C, white stands for $R < 0.1$, light gray for $0.1 \leqslant R < 0.5$ and dark gray for $R \geqslant 0.5$. Robustness increases with R ($R \in [0,1]$; Materials and methods). For proteins, results apply only for gradients formed with very unstable mRNAs.

whereas the differential expression of gradients driven by cell lineage transport becomes robust, their timing of formation becomes extremely sensitive to variations in the cell cycle (Figure 5A and C).

Therefore, for gradients involving nonlinear growth with repeated divisions and dilutions, our analysis revealed that the differential spatial domains of expression become less sensitive to alterations in the duration of the cell cycle, but at the expense of more variable timing in gradient formation. In contrast, gradients not involving repeated dilution of the molecular content have a fixed timing of gradient formation but a non-robust differential expression for changes in the duration of the cell cycle.

A *Hoxd13* gradient in the vertebrate limb created by cell lineage transport

Until now, no mRNA gradient involving clonal dilution and transport of the molecular content driven by evenly proliferating cells has been reported in a developing embryo. Therefore, we searched for an example of a developmental scenario where cell lineage transport could elicit a gradient.

The early stages of the chick limb are characterized by the outgrowth and elongation of the initial limb bud. During these early stages, it has been readily demonstrated that cells proliferate evenly all over the limb bud (Hornbruch and Wolpert, 1970; Vargesson *et al*, 1997; Sun *et al*, 2002). Moreover, cell tracing experiments have shown that the spatial distribution of descendants of cells located distally at early stages form an elongated shape along the proximo-distal axis (Supplementary Figure S4A; Vargesson *et al*, 1997; Dudley *et al*, 2002). Therefore, the vertebrate limb bud has appropriate morphogenetic dynamics to analyze if mRNA gradients are formed during early development according to cell lineage transport dynamics involving clonal dilution.

Hox genes are known to play critical roles during vertebrate limb patterning and outgrowth (Dolle *et al*, 1993; Davis and Capecchi, 1994; Morgan and Tabin, 1994; Fromental-Ramain *et al*, 1996; Goff and Tabin, 1997; Heanue *et al*, 1997; Shubin *et al*, 1997; Zakany *et al*, 2004; Kmita *et al*, 2005). *Hoxd13*, in particular, is the most 5′-*Hoxd* gene and is shown to be necessary for proper development of the autopod in vertebrates. Moreover, it has been shown that *Hoxd13* can trigger the appearance of digits (Kmita *et al*, 2005). *Hoxd13* shows a dynamic and restricted expression pattern in the developing limb (Nelson *et al*, 1996). Initially, *Hoxd13* expression is restricted to the distal posterior region (Hamburger and Hamilton stages 19–22) and, later on, it extends anteriorly within the distal domain (Hamburger and Hamilton, 1951; Nelson *et al*, 1996). Importantly, cell fate analyses have revealed that the dynamic expression pattern of *Hoxd13* can be understood in terms of the expansion of former *Hoxd13*-expressing cells (Vargesson *et al*, 1997). For the purpose of this paper, we focused only on characterizing whether *Hoxd13* expression is graded and driven by cell lineage transport. Owing to the correlation of its expression with autopod development, we expect that our characterization of *Hoxd13* expression formation will be able to give some hints to future work on the specific function of this gene, which still requires further elucidation.

As shown in our previous analyses, cell lineage gradients require a DoT. We reasoned that in the limb bud the DoT should be located preferentially on the distal end (see Discussion). According to previous cell fate analyses on distally located cells (Supplementary Figure S4B; Vargesson *et al*, 1997), we inferred that cell descendants of the DoT would be located along the proximo-distal axis, with older cells found more proximally, able to potentially elicit a distal-to-proximal cell lineage mRNA gradient. As previously described, if such a gradient is formed, the intronic domain of expression would be located at the distal end, whereas the exonic signal will be graded and will span over a domain much larger and extending more proximally than the intronic expression.

By reverse transcription–PCR (RT–PCR) analysis, we confirmed intronic expression of *Hoxd13* in the distal region of the limb bud in both forelimbs and hindlimbs during stages 21–26 (Figure 6A and Supplementary Figures S3 and S4B; data not shown). This expression did not exhibit any significant graded profile (data not shown), discarding the potential emergence of an mRNA gradient through graded transcription. The width (along the proximo-distal axis) of the intronic expression increased at stage 25, especially in the hindlimb (Figure 6A and Supplementary Figure S4B; data not shown).

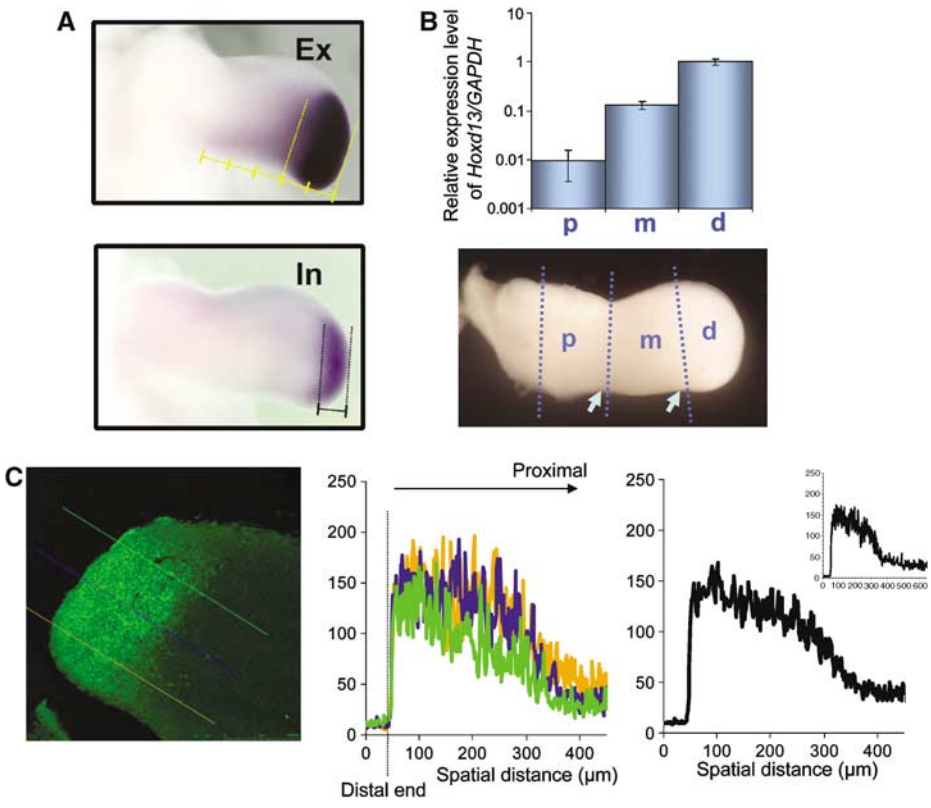

Figure 6 Gradient of *Hoxd13* mRNA in the chick limb bud. (**A**) Whole-mount *in situ* hybridization of (Ex) exonic and (In) intronic expression domains in the forelimb at stage 26. Panels are at the same magnification. Lines compare the length of the exonic and intronic expression domains. (**B**) qPCR for mRNA *Hoxd13* in (p) proximal, (m) medial and (d) distal regions in logarithmic scale. The relative amount has been normalized to the value at the distal region. The bottom picture depicts the three spatial regions over the limb bud. Arrows denote the wrist and elbow. (**C**, left) Fluorescent *in situ* hybridization section of *Hoxd13*. The signal has been analyzed along the proximo-distal axis at different antero-posterior positions (represented by lines). (C, middle) Average fluorescent signal along the proximo-distal axis at (green) posterior, (blue) medial and (orange) anterior positions. (C, right) Total average fluorescent signal along the proximo-distal axis. The inset depicts the average gradient over longer distances.

Whole-mount *in situ* hybridization depicted an exonic domain of expression much larger and spanning more proximally than the intronic domain of expression (Figure 6A and Supplementary Figure S4B), pinpointing where a gradient of *Hoxd13* formed by cell lineage transport could be present. Specifically, our data revealed that exonic expression extends over the spatial region potentially occupied by former transcribing cells at the intronic domain (Materials and methods).

A graded expression of *Hoxd13* was first confirmed qualitatively by *in situ* hybridization and semiquantitative RT–PCR, showing a higher level of exonic expression at the distal end, as expected (Supplementary Figure S4C; data not shown). Quantitative PCR (qPCR) on three (proximal, medial and distal) regions of the chick limb bud, normalized to the housekeeping gene Gapdh (Materials and methods), clearly evidenced such a gradient and indicated a 10-fold decay between the most distal and medial regions (Figure 6B). Fluorescent *in situ* hybridization signal (Materials and methods), despite not being linearly proportional to the real mRNA gradient owing to enzymatic amplification, further confirmed the existence of a distal-to-proximal *Hoxd13* gradient. We note that the graded fluorescent signal in anterior and posterior regions of distal and middle regions was rather similar (Figure 6C). From the quantitative data on the graded expression of *Hoxd13* at stage 25 obtained by qPCR (Figure 6B) and using our mathematical model, we could estimate the molecular half-life of *Hoxd13*. Our results indicate a range of relative half-lives $\gamma_m \approx 0.3–0.8$ (Materials and methods), which for cell cycles between 8 and 12 h (Vargesson *et al*, 1997) corresponds to half-lives in the range of 2.4–9.6 h. As expected, the differential size between exonic and intronic domains of expression at stage 25 also supported a relative half-life within this range (Materials and methods).

Altogether, our results indicate that *Hoxd13* expression in the chick limb bud is graded and pinpoints cell lineage transport as the mechanism driving such gradient formation. We expect future work to elucidate whether other *Hox* genes exhibit similar graded expressions and how limb development depends on them.

Discussion

Gradients of secreted proteins transported through different molecular mechanisms have been extensively analyzed in developmental biology. Generally, these mechanisms of gradient formation do not take into account the spatiotemporal dynamics of cells or the mRNA dynamics (Zhu and Scott,

2004). Here we have shown a full mathematical framework, which for the first time takes into account the dynamics of cells, mRNAs and proteins, and we have provided new experimental evidence for a less understood mechanism of gradient formation that might prove to play an important role during embryo development. In this mechanism, cells act as the carriers of molecules such as mRNAs and non-secreted proteins, and, through cell division, dilute this molecular content over their progeny. Our model shows how this cell lineage transport mechanism can elicit mRNA gradients, which in turn create gradients of non-secreted proteins. In addition, our results indicate that cell lineage transport can account as well for the formation of non-secreted protein gradients from local sources of protein translation not involving graded distributions of mRNA.

One of the interesting features of the cell lineage transport mechanism resides in its ability to generate gradients of non-secreted molecules, such as receptors, transcription factors and second messengers (mRNA, microRNA, etc.), indicating that not only secreted proteins, but also non-secreted proteins, should be the focus of studying biologically relevant graded molecular distributions. In addition, cell lineage transport could also participate in the formation of gradients of secreted proteins. Accordingly, the mathematical framework presented herein can be extended to secreted proteins by introducing the appropriate molecular transport dynamics (diffusion, vesicle trafficking, etc.).

Our results exemplify how cell proliferation and cell growth can elicit molecular gradients solely by diluting the molecular content, without requiring any molecular degradation. In contrast, our results showed that the molecular turnover becomes essential in forming a gradient when cell proliferation occurs only in a pool of mRNA transcribing cells, as previously reported (Gaunt *et al*, 2003; Dubrulle and Pourquié, 2004; Gaunt, 2004). Through our theoretical analysis, we have uncovered that these diverse tissue dynamics elicit gradients exhibiting very different profiles that lead to specific spatial and temporal sensitivities under changes of the duration of the cell cycle.

The present study has focused on a proliferating population of cells whose descendants become located one next to another creating an elongated structure. However, our mathematical framework could be extended to growing morphologies that involve cell rearrangements, intermingling or migration. In this case, the critical parameter characterizing the cell dynamics would be the timing of the spatial displacements of cells, which would involve the dynamics of the cell cycle. In addition, our mathematical framework could be extended to growing populations of cells that do not distribute along a specific spatial axis but which have a fixed DoT. In all these cases, we can expect the formation of gradients driven by cell lineage transport, as long as younger cells become located on average closer to the DoT than older cells. These gradients are expected to exhibit spatial fluctuations, like gradients emerging from non-constant cell cycles. In all these scenarios, and in order to buffer such fluctuations, pattern formation could occur through the integration of the graded signal in neighboring cells.

The mechanism underlying cell lineage transport implies that gradients are formed only over the progeny of a pool of cells, that is, those initially at the DoT. In most invertebrate species, embryonic structures emerge from cells genealogically related, producing lineage-based cellular patterning. In these cases, the formation of mRNA and protein gradients through cell lineage transport might be an important mechanism of pattern formation. In contrast, in early development of vertebrate embryos, cell dispersal is present in many instances, as revealed by clonal analyses in mouse, *Xenopus*, fish and chick embryos, leading to embryonic structures that arise from cells that do not descend from a common progenitor (Mathis and Nicolas, 2002). This implies that the formation of relevant cell lineage mRNA and protein gradients in vertebrate embryos might be restricted to very local structures, such as the limbs, for instance, and, possibly, not as common as in invertebrates.

An essential element for the formation of gradients driven by cell lineage transport is the presence of a local domain of mRNA transcription (the DoT) that contains proliferating cells. This domain might be sustained by signals coming from surrounding tissues, like those coming from the apical ectodermal ridge for mesenchymal cells in the vertebrate limb bud. Note that the DoT could be thought of as acting as a kind of niche of stem cells: cells are actively proliferating and self-renewing such that some of the progeny remains at the DoT and the rest of the progeny is displaced outside the DoT through oriented cell division, for instance (Yamashita *et al*, 2003).

A major question in developmental biology is the coordination between patterning and growth. Gradient formation of secreted proteins has been proposed to pattern developing embryos and control the growth of a tissue through its steepness (Lawrence, 2001). As gradients driven by cell lineage transport are formed as tissue grows, linking the timing of mitotic divisions with the steepness of the gradient, cell lineage transport gradients might represent a mechanism that coordinates the dynamics of patterning and growth.

Materials and methods

Analytical gradient profiles of gradients driven by cell lineage transport

Our simulations start with N cells located at the DoT ($x \in [0, Nl-l]$; Supplementary information). Thus, when all cells divide in synchrony, the spatial dynamics of the cell furthest away from the DoT is given by $x_\tau = 2^\tau Nl - l$, where τ indicates the total number of cell divisions, with cell cycle Cc. From the equations in Figure 1, the amount of mRNA and protein inside this cell as a function of the amounts of mRNA and protein its progenitor had at the DoT just before dividing and letting its descendant outside this domain (m_0 and p_0, respectively) is given by

$$m_\tau = \alpha^\tau m_0 2^{-\tau Cc/H_m} \tag{1a}$$

$$p_\tau = b\left(\frac{2^{-\tau Cc/H_p} - 2^{-\tau Cc/H_m}}{H_m^{-1} - H_p^{-1}}\right)\frac{\alpha^\tau m_0}{\ln 2} + \alpha^\tau p_0 2^{-\tau Cc/H_p}; \quad H_m \neq H_p \tag{1b}$$

$$p_\tau = \alpha^\tau b \tau Cc\, m_0 2^{-\tau Cc/H} + \alpha^\tau p_0 2^{-\tau Cc/H}; \quad H_m = H_p \equiv H \tag{1c}$$

where U=Cc has been introduced. By introducing the spatial position of this cell in equations (1a–c), we obtained a continuous expression for the gradient profile at times just before another cell divided:

$$m(x) = m_0\left(\frac{x}{Nl}+\frac{1}{N}\right)^{-1-(1/\gamma_m)} \tag{2a}$$

$$p(x) = \frac{bm_0}{(\ln 2/H_m - \ln 2/H_p)}\left(\left(\frac{x}{Nl}+\frac{1}{N}\right)^{-1-(1/\gamma_p)} - \left(\frac{x}{Nl}+\frac{1}{N}\right)^{-1-(1/\gamma_m)}\right) + p_0\left(\frac{x}{Nl}+\frac{1}{N}\right)^{-1-(1/\gamma_p)} \quad ; \quad H_m \neq H_p \tag{2b}$$

$$p(x) = \left(\frac{x}{Nl}+\frac{1}{N}\right)^{-1-(1/\gamma)} \times \left(p_0 + \left(\log_2\left(\frac{x}{Nl}+\frac{1}{N}\right)\right)\mathrm{Cc} \equiv m_0 b\right); \quad H_m = H_p \equiv H \tag{2c}$$

for $x > Nl - l$ and where α=0.5 and $\gamma_{m,p} \equiv H_{m,p}/\mathrm{Cc}$ has been set.

As shown in Figure 2 and Supplementary Figure S1, these analytical profiles correctly fit the numerical gradients, obtained either for synchronous or non-synchronous cell divisions, and fluctuating cell cycles and/or inherited fractions of the molecular content.

For very small relative half-lives (short mRNA half-lives compared to the cell cycle, $\gamma_m \ll 1$), no mRNA gradient is created ($m(x > Nl - l) \overset{\gamma_m \to 0}{\longrightarrow} 0$) but still a protein gradient can be formed. In this case, only the cells in the DoT translate the protein and thus the DoT becomes the unique source of protein translation. This protein gradient is characterized by the single power-law decay of equation (2a) ($p(x > Nl - l) \overset{\gamma_m \to 0}{\longrightarrow} p_0((x+l)/Nl)^{-1-1/\gamma_p}$).

The analytical results derived from these profiles were computed with Mathematica software (Wolfram Research Inc.).

Length, number of divisions and time

Herein we derive the spatial and temporal properties of mRNA cell lineage gradients. As, as indicated, protein gradients formed by non-graded mRNAs exhibit a single power-law profile, equivalent mathematical expressions to those for mRNAs apply for protein gradients (Table I).

The spatial extent of the mRNA gradient was defined as $L_{10}^m = x_{10}^m + l$ where x_{10}^m is the spatial position where the gradient has decayed 10-fold ($m(x_{10}^m) = m_0/10$, with m_0 being the constant amount of mRNA at the DoT, and $m(x)$ is given by equation (2a)). For other choices of decay of the gradient (q-fold decays), we have $m(x_q^m) = m_0/q$, which leads to $L_q^m = Nlq^{1/(1+\mathrm{Cc}/H_m)}$. Note that the extent of mRNA gradients increases proportionally to the number N of progenitor cells at the DoT and the cell diameter l, as expected, and saturates to $L_{10}^m \overset{\gamma_m \to \infty}{\longrightarrow} qNl$. The spatial extent of protein gradients can be analogously computed, although no closed analytical expression can be obtained when the mRNA is distributed in a graded profile (Supplementary information).

The average number of divisions per cell at the DoT required for creating an mRNA or protein gradient through cell lineage transport with a q-fold decay satisfies $ND_q^{m,p} = \log_2(L_q^{m,p}/L^I)$, where the nonlinear growth of the tissue has been taken into account (Table I and Supplementary information). Once cells at the DoT have started dividing, the time required for the formation of a gradient with a q-fold decay is given by $t = ND_q^{m,p}\,\mathrm{Cc}$ (Table I). Note $t \overset{H_{m,p}/\mathrm{Cc} \to \infty}{\longrightarrow} \mathrm{Cc}\log_2 10$ for 10-fold decay gradients.

The derivation of these properties for gradients that do not involve clonal dilution is detailed in Supplementary information.

A measure for robustness and sensitivity

We quantified the robustness R of a property or function F under changes in the variable X as $R = h/(h + \Delta_r F/\Delta_r X)$, where Δ is the magnitude of the change of X, $\Delta_r X = \Delta/X$ is the relative change and $\Delta_r F = (F(X+\Delta) - F(X))/F(X)$ characterizes the sensitivity of F. We set h=0.1. Note that R ranges between 0 and 1, R=1 (R=0) corresponding to robust (non-robust) dynamics. Therefore, robustness emerges for low sensitivities of F ($h^{-1}\Delta_r F/\Delta_r X \ll 1$). This measure of robustness was applied to the differential expression ($F = L_{10}^m/L^I$) and to the time needed to form a gradient ($F = t$) under changes in the duration of the cell cycle (X=Cc). For $F = L_{10}^m/L^I$, we measured how the sensitivity changed when clonal dilution was participating. Accordingly, we took the ratio between the sensitivity S_d for gradients driven by cell lineage transport involving clonal dilution owing to cell proliferation and the sensitivity S_{nd} for gradients that had proliferating cells only at the DoT and thus did not involve massive dilution ($S_d/S_{nd} = \Delta_r F(\text{dilution})/\Delta_r F(\text{no dilution})$). $S_d/S_{nd} < 1$ indicates that dilution decreases the sensitivity to changes in the duration of the cell cycle of the differential domains of expression.

Hoxd13 expression in the chick limb bud

Whole-mount *in situ* hybridization was carried out according to standard procedures (Wilkinson, 1993). The chick *Hoxd13* exon probe contains 1.2 kb 3′-UTR. To clone an intron region of the chick *Hoxd13* gene, we found the *Hoxd* cluster on chromosome 7 in the NCBI database. The second intron (590 bp) was amplified by PCR from chick genomic DNA, subcloned into pCR-II (Invitrogen) and confirmed by nucleotide sequencing.

Fluorescent *in situ* hybridization

Chick forelimbs at stage 25/26 were sectioned at 10 μm after paraffin embedding. *In situ* hybridization was performed using standard procedures (Izpisua-Belmonte *et al*, 1991) coupled to the TSA fluorescence system according to the manufacturer's instructions (Perkin Elmer), and *Hoxd13* mRNA was detected as deposited fluorescent signal by the TSA fluorescence system.

Fluorescent images were analyzed by Leica SP5 tandem-AOBS_MP multiphoton laser microscope with software AFS Leica. The intensity was quantified along the proximo-distal axis on four different limb sections. The total average gradient profile was obtained from the data of nine gradients. The signal over longer distances along the proximo-distal axis was averaged over four gradients. The average was computed by setting the distal end of all gradients at the same spatial position.

Quantitative PCR

Chick forelimb buds from stage 25/26 embryos were dissected into distal, medial and proximal regions (Figure 6B). One sample consisted of 5–6 forelimbs, and five samples for the distal, middle and proximal were used for the analysis. Total RNA was isolated by using Trizol (Invitrogen) according to the manufacturer's instructions. cDNA was synthesized with 3 μg of total RNA with the Superscript II and oligo(dT) primer (Invitrogen), and used after 10-fold dilution in order to monitor PCR products in the range of a relative standard curve. qPCR analysis was performed with the SYBR green system according to the manufacturer's instructions (Applied Biosystems) with a two-step PCR amplification program (10 min at 95°C followed by 40 cycles of 15 s at 95°C, 45 s at 53°C). A relative standard curve was constructed using 10-fold serial dilutions of cDNA derived from distal limb buds at stage 24–26. Data were calculated based on the threshold cycle, where the SYBR green signal becomes higher than that of the background. For quantitative comparison of gene expression, the relative expression level of *Hoxd13* against *GAPDH* was calculated. The following primers for chick *Hoxd13* were used: sense 5′-AGACATGGTCT CAACGTTTGGC and antisense 5′-GCACATCTCGGGCTGGTTTAG. For *GAPDH*, we used the following primers: sense 5′-GGACACTTCAAGGG CACTGT and antisense 5′-GGTGAAGACACCAGTGGACT. The amplification product sizes are 193 and 150 bp for *Hoxd13* and *GAPDH*, respectively.

Hoxd13 expression in terms of the cell lineage transport model

Our data support that *Hoxd13* exonic expression spans within the region potentially occupied by cell descendants of the intronic domain. *Hoxd13* expression starts at stages 18/19 (Nelson *et al*, 1996), and the limb takes 12–19 h to develop to stage 22 (Hamburger and Hamilton, 1951). As the duration of the cell cycle during limb development has been reported as 8–12 h (Vargesson *et al*, 1997), cell descendants of the intronic domain (DoT) are expected to extend up to a region at most five times larger than the DoT. Therefore, at stages 21/22, we expected an exonic domain of expression at most five times larger than the intronic one, as we found indeed (n=4 limbs (intron), n=12 limbs (exon); Supplementary Figure S4B). Similar conclusions can be obtained from the expression patterns at later stages. In addition, these results are in agreement with previously reported correlations between exonic *Hoxd13* expression and cell lineage analysis in the chick limb bud (Vargesson *et al*, 1997).

qPCR measured the amount of mature mRNA over a spatial region. In terms of the cell lineage transport model, the total amount at the distal region, which extends over a region $1+\varepsilon$ times the intronic domain's length, is $M_D = \int_D m(x)\mathrm{d}x = Nlm_0(1+\gamma_m[1-(1+\varepsilon)^{-1/\gamma_m}])$, whereas the total amounts at the medial and proximal regions are respectively $M_M = Nlm_0\gamma_m((1+\varepsilon)^{-1/\gamma_m} - (2+2\varepsilon)^{-1/\gamma_m})$ and $M_P = Nlm_0\gamma_m((2+2\varepsilon)^{-1/\gamma_m} - (3+3\varepsilon)^{-1/\gamma_m})$, assuming all regions have the same size. Thus, $M_M/M_P = (2^{1/\gamma_m}-1)/(1-(2/3)^{1/\gamma_m})$ and, using the value indicated by the qPCR, we obtained $\gamma_m \approx 0.3$. From M_M/M_D and setting $\varepsilon \leqslant 1$ (Figure 6A and B), we obtained $\gamma_m \leqslant 0.8$. Note that this value is lowered if we take into account that in proximal regions, the exonic expression does not extend over the whole antero-posterior axis.

qPCR could not be performed at earlier stages owing to the small size of limbs. Assuming a 10-fold decay over the exonic region, from the ratio between exonic and intronic expression domains (Figure 6A and Supplementary Figure S4B) and identifying this ratio as L^m_{10}/L^I, we could estimate a plausible range of relative half-lives, as well, through $\gamma_m = (1/\log_{10}(L^m_{10}/L^I) - 1)^{-1}$. At stage 25/26, we had $L^m_{10}/L^I \approx 1, 2$ (n=6 limbs (intron), n=6 limbs (exon)), which lead to $\gamma_m \approx 0.45$, which is in agreement with the previous analysis. At stage 21/22, we had $L^m_{10}/L^I \approx 3, 4$ (n=4 limbs (intron), n=12 limbs (exon)), which lead to $\gamma_m \approx 0.9, 1.5$. A decrease in the relative half-lives during limb development could result from an increase in the cell cycle, which is supported by previously reported data on the mitotic index (Hornbruch and Wolpert, 1970).

Supplementary information

Supplementary information is available at the *Molecular Systems Biology* website (www.nature.com/msb).

Acknowledgements

We thank Concepción Rodríguez-Esteban, Mercè Martí, Joaquin Rodríguez-León, Hiroko Kawakami and Carolina Soler for their help with experiments and embryo pictures. We also thank the late Francis Crick, Marcos González-Gaitán and Javier Capdevila for their helpful insights at the early stages of this work. MI has been partially supported by the Fulbright Program and Generalitat of Catalunya and by the Ramon y Cajal Program from the Spanish Ministerio de Educación y Ciencia. This work was supported by grants from the Human Frontiers Science Program, the NIH, BBVA, Fundacion Cellex and the G Harold and Leila Y Mathers Charitable Foundation.

References

Bhalerao RP, Bennett MJ (2003) The case for morphogens in plants. *Nat Cell Biol* **5:** 939–943

Bollenbach T, Kruse K, Pantazis P, Gonzalez-Gaitan M, Julicher F (2005) Robust formation of morphogen gradients. *Phys Rev Lett* **94:** 018103

Conlon I, Raff M (1999) Size control in animal development. *Cell* **96:** 235–244

Crick F (1970) Diffusion in embryogenesis. *Nature* **225:** 420–422

Davis AP, Capecchi MR (1994) Axial homeosis and appendicular skeleton defects in mice with a targeted disruption of hoxd-11. *Development* **120:** 2187–2198

Dolle P, Dierich A, LeMeur M, Schimmang T, Schuhbaur B, Chambon P, Duboule D (1993) Disruption of the Hoxd-13 gene induces localized heterochrony leading to mice with neotenic limbs. *Cell* **75:** 431–441

Driever W, Nusslein-Volhard C (1988a) A gradient of bicoid protein in *Drosophila* embryos. *Cell* **54:** 83–93

Driever W, Nusslein-Volhard C (1988b) The bicoid protein determines position in the *Drosophila* embryo in a concentration-dependent manner. *Cell* **54:** 95–104

Dubrulle J, Pourquié O (2004) fgf8 mRNA decay establishes a gradient that couples axial elongation to patterning in the vertebrate embryo. *Nature* **427:** 419–422

Dudley AT, Ros MA, Tabin CJ (2002) A re-examination of proximodistal patterning during vertebrate limb development. *Nature* **418:** 539–544

Eldar A, Dorfman R, Weiss D, Ashe H, Shilo BZ, Barkai N (2002) Robustness of the BMP morphogen gradient. *Nature* **419:** 304–308

Eldar A, Rosin D, Shilo BZ, Barkai N (2003) Self-enhanced ligand degradation underlies robustness of morphogen gradients. *Dev Cell* **5:** 635–646

Entchev EV, Schwabedissen A, Gonzalez-Gaitan M (2000) Gradient formation of the TGF-beta homolog Dpp. *Cell* **103:** 981–991

Ephrussi A, St Johnston D (2004) Seeing is believing: the bicoid morphogen gradient matures. *Cell* **116:** 143–152

Figueroa A, Cuadrado A, Fan J, Atasoy U, Muscat GE, Munoz-Canoves P, Gorospe M, Munoz A (2003) Role of HuR in skeletal myogenesis through coordinate regulation of muscle differentiation genes. *Mol Cell Biol* **23:** 4991–5004

Fromental-Ramain C, Warot X, Messadecq N, LeMeur M, Dolle P, Chambon P (1996) Hoxa-13 and Hoxd-13 play a crucial role in the patterning of the limb autopod. *Development* **122:** 2997–3011

Gaunt SJ (2004) Morphogen gradients formed by decay. *BioEssays* **26:** 1143

Gaunt SJ, Drage D, Cockley A (2003) Vertebrate caudal gene expression gradients investigated by use of chick cdx-A/lacZ and mouse cdx-1/lacZ reporters in transgenic mouse embryos: evidence for an intron enhancer. *Mech Dev* **120:** 573–586

Goff DJ, Tabin CJ (1997) Analysis of Hoxd-13 and Hoxd-11 misexpression in chick limb buds reveals that Hox genes affect both bone condensation and growth. *Development* **124:** 627–636

Greco V, Hannus M, Eaton S (2001) Argosomes: a potential vehicle for the spread of morphogens through epithelia. *Cell* **106:** 633–645

Green J (2002) Morphogen gradients, positional information, and *Xenopus*: interplay of theory and experiment. *Dev Dyn* **225:** 392–408

Gurdon JB, Bourillot PY (2001) Morphogen gradient interpretation. *Nature* **413:** 797–803

Hamburger V, Hamilton HL (1951) A series of normal stages in the development of the chick embryo. *J Morphol* **88:** 49–92

Heanue TA, Johnson RL, Izpisua-Belmonte JC, Stern CD, De Robertis EM, Tabin CJ (1997) Goosecoid misexpression alters the morphology and Hox gene expression of the developing chick limb bud. *Mech Dev* **69:** 31–37

Hornbruch A, Wolpert L (1970) Cell division in the early growth and morphogenesis of the chick limb. *Nature* **226:** 764–766

Houchmandzadeh B, Wieschaus E, Leibler S (2002) Establishment of developmental precision and proportions in the early *Drosophila* embryo. *Nature* **415:** 798–802

Izpisua Belmonte JC, Tickle C, Dolle P, Wolpert L, Duboule D (1991) Expression of the homeobox Hox-4 genes and the specification of position in chick wing development. *Nature* **350:** 585–589

Kerszberg M, Wolpert L (1998) Mechanisms for positional signalling by morphogen transport: a theoretical study. *J Theor Biol* **191:** 103–114

Kmita M, Tarchini B, Zakany J, Logan M, Tabin CJ, Duboule D (2005) Early developmental arrest of mammalian limbs lacking HoxA/HoxD gene function. *Nature* **435:** 1113–1116

Kruse K, Pantazis P, Bollenbach T, Julicher F, Gonzalez-Gaitan M (2004) Dpp gradient formation by dynamin-dependent endocytosis: receptor trafficking and the diffusion model. *Development* **131:** 4843–4856

Lander AD, Nie Q, Wan FY (2002) Do morphogen gradients arise by diffusion? *Dev Cell* **2:** 785–796

Lawrence PA, Struhl G (1996) Morphogens, compartments, and pattern: lessons from *Drosophila*? *Cell* **85:** 951–961

Lawrence PA. (2001) Morphogens: how big is the big picture? *Nat Cell Biol* **3:** E151–E154

Lecuit T, Cohen SM (1998) Dpp receptor levels contribute to shaping the Dpp morphogen gradient in the *Drosophila* wing imaginal disc. *Development* **125:** 4901–4907

Mann RS, Culi J (2005) Developmental biology: morphogens hitch a greasy ride. *Nature* **435:** 30–33

Martinez Arias A (2003) Wnts as morphogens? The view from the wing of *Drosophila*. *Nat Rev Mol Cell Biol* **4:** 321–325

Mathis L, Nicolas JF (2002) Cellular patterning of the vertebrate embryo. *Trends Genet* **18:** 627–635

Morgan BA, Tabin C (1994) Hox genes and growth: early and late roles in limb bud morphogenesis. *Dev Supp* **l:** 181–186

Nelson CE, Morgan BA, Burke AC, Laufer E, DiMambro E, Murtaugh LC, Gonzales E, Tessarollo L, Parada LF, Tabin C (1996) Analysis of Hox gene expression in the chick limb bud. *Development* **122:** 1449–1466

Panakova D, Sprong H, Marois E, Thiele C, Eaton S (2005) Lipoprotein particles are required for Hedgehog and Wingless signalling. *Nature* **435:** 58–65

Peltz SW, Brewer G, Bernstein P, Hart PA, Ross J (1991) Regulation of mRNA turnover in eukaryotic cells. *Crit Rev Eukaryot Gene Expr* **1:** 99–126

Pfeiffer S, Alexandre C, Calleja M, Vincent JP (2000) The progeny of wingless-expressing cells deliver the signal at a distance in *Drosophila* embryos. *Curr Biol* **10:** 321–324

Pfeiffer S, Ricardo S, Manneville JB, Alexandre C, Vincent JP (2002) Producing cells retain and recycle Wingless in *Drosophila* embryos. *Curr Biol* **12:** 957–962

Ramirez-Weber FA, Kornberg TB (1999) Cytonemes: cellular processes that project to the principal signaling center in *Drosophila* imaginal discs. *Cell* **97:** 599–607

Ross J (1995) mRNA stability in mammalian cells. *Microbiol Rev* **59:** 423–450

Sachs AB (1993) Messenger RNA degradation in eukaryotes. *Cell* **74:** 413–421

Shimmi O, Umulis D, Othmer H, O'Connor MB (2005) Facilitated transport of a Dpp/Scw heterodimer by Sog/Tsg leads to robust patterning of the *Drosophila* blastoderm embryo. *Cell* **120:** 873–886

Shubin N, Tabin C, Carroll S (1997) Fossils, genes and the evolution of animal limbs. *Nature* **388:** 639–648

Strigini M, Cohen SM (2000) Wingless gradient formation in the *Drosophila* wing. *Curr Biol* **10:** 293–300

Sun X, Mariani FV, Martin GR (2002) Functions of FGF signalling from the apical ectodermal ridge in limb development. *Nature* **418:** 501–508

Tabata T (2001) Genetics of morphogen gradients. *Nat Rev Genet* **2:** 620–630

Tanaka Y, Okada Y, Hirokawa N (2005) FGF-induced vesicular release of Sonic hedgehog and retinoic acid in leftward nodal flow is critical for left–right determination. *Nature* **435:** 172–177

Teleman AA, Cohen SM (2000) Dpp gradient formation in the *Drosophila* wing imaginal disc. *Cell* **103:** 971–980

Teleman AA, Strigini M, Cohen SM (2001) Shaping morphogen gradients. *Cell* **105:** 559–562

Turing AM (1952) The chemical basis of morphogenesis. *Proc R Soc London B* **237:** 37–72

Vargesson N, Clarke JD, Vincent K, Coles C, Wolpert L, Tickle C (1997) Cell fate in the chick limb bud and relationship to gene expression. *Development* **124:** 1909–1918

Varshavsky A (1996) The N-end rule: functions, mysteries, uses. *Proc Natl Acad Sci USA* **93:** 12142–12149

Vincent JP, Dubois L (2002) Morphogen transport along epithelia, an integrated trafficking problem. *Dev Cell* **3:** 615–623

Wilkinson DG (1993) Whole mount in situ hybridization of vertebrate embryos. In *In Situ Hybridization: A Practical Approach*, Wilkinson DG (ed) pp 75–83. Oxford: Oxford University Press

Wolpert L (1969) Positional information and spatial pattern of cellular differentiation. *J Theor Biol* **25:** 1–47

Yamashita YM, Jones DL, Fuller MT (2003) Orientation of asymmetric stem cell division by the APC tumor suppressor and centrosome. *Science* **301:** 1547–1550

Zakany J, Kmita M, Duboule D (2004) A dual role for Hox genes in limb anterior–posterior asymmetry. *Science* **304:** 1669–1672

Zhu AJ, Scott MP (2004) Incredible journey: how do developmental signals travel through tissue? *Genes Dev* **18:** 2985–2997